Analytical and Experimental Studies of Nonlinear Transient Responses of Stiffened Cylindrical Panels

Richard W. H. Wu* and Emmett A. Witmer†
Massachusetts Institute of Technology, Cambridge, Mass.

A solution procedure which employs the spatial finite-element method together with the temporal finite-difference method is presented for predicting transient elastic-plastic large-deflection responses of structures. The assumed-displacement finite-element formulation is described in detail for quadrilateral cylindrical panel elements stiffened orthogonally by longitudinal and/or circumferential stiffeners. The sheet high-explosive loading technique was employed to conduct impulsive loading and structural response tests of circumferentially stiffened cylindrical panels of 6061-T6 aluminum alloy, with all four edges clamped. Large transient and permanent structural deformations were produced. Excellent theoretical/experimental correlation for transient strains and permanent deformation is observed.

I. Introduction

THERE are many situations of practical interest in which structures are subjected to transient loading of high intensity which induces transient deformations ranging from small-deflection linear-elastic to large-deflection elastic-plastic and permanent deformations. Situations of this type include various flight, water, and land vehicles and stationary structures which are subjected to blast, impact, collision, etc. Also of interest is the forming of simple and complex structural shapes by using explosive and/or magnetic devices.

While the prediction of small-deflection linear-elastic responses can readily be accomplished by numerous analytical or approximate methods, the prediction of large-deflection elastic-plastic transient and permanent responses is much more difficult because of the important presence of strong geometric and material-property nonlinearities. Various means of analysis to predict the latter "more complicated" behavior have been devised. Among them, the two most general and versatile methods are the finite-difference method and the finite-element method. For predicting large-deflection elastic-plastic transient response behavior of beams, rings, plates, and thin shells, finite-difference solutions are reported for example, in Refs. 1-8; similar finite-element predictions are reported in Refs. 9-12. Of the two methods, the finite-element method is generally considered to be very effective and convenient for analyzing a continuum with a complicated geometric shape, material properties, and boundary conditions; on the other hand, for analyzing a continuum with smoothly-varying properties and geometric shape, the finite-difference method may turn out to be more efficient, especially if only transient deflections are to be predicted.

Since geometrically-stiffened structures are often of common practical interest in design, application of the finite-element method is extended in the present study to analyze the large-deflection elastic-plastic transient responses of stiffened cylindrical panels, thereby enabling one to exploit the geometric versatility advantages of the finite-element method.

Received September 26, 1974; revision received December 23, 1974; presented as Paper 75-810 at the AIAA/ASME/SAE 16th Structures, Structural Dynamics, and Materials Conference, Denver, Colorado, May 27-29, 1975. This work was supported by the Army Materials and Mechanics Research Center under Contract DAAG46-72-C-0212. The authors wish to acknowledge the assistance of F. Merlis of the MIT-ASRL in carrying out the experiments.

Index category: Structural Dynamic Analysis.

*Senior Research Engineer, Aeroelastic and Structures Research Laboratory (ASRL); currently with General Electric Company, Nuclear Energy Division. Member AIAA.

†Professor of Aeronautics and Astronautics. Member AIAA.

To determine whether methods of analysis provide accurate and reliable predictions for large-deflection elastic-plastic transient and permanent structural responses, it is essential that they be expressed by carrying out detailed comparisons of predictions against pertinent definitive experimental data. High-quality experimental data on beams and rings are reported in Refs. 13-15, and on plates and shells in Refs. 16-20; all of these experiments were conducted on unstiffened specimens. Since the available experimental data are only for unstiffened structures, experiments of impulsively loaded circumferentially-stiffened cylindrical panels of 6061-T6 aluminum alloy with all four edges clamped have been carried out.[21] Brief descriptions of the experimental procedure and the results for these stiffened models are given in this paper.

For generality and clarity in presentations, the equations which govern the large-deflection elastic-plastic transient responses of a solid continuum are presented in three-dimensional tensor form, and the indicial notation and summation convention associated with vector and tensor analysis are used. These equations are then specialized to treat stiffened cylindrical-shell problems. Comparisons of predicted responses for a stiffened-quadrilateral-cylindrical panel which is subjected to initial impulsive loading are made with experimental results.

II. Formulation of the Governing Equations

A. Spatial Finite-Element Approximation

In the spatial finite-element approximation, the continuum is subdivided conceptually into a finite number of elements. Considering the continuum in equilibrium, the Principle of Virtual Work states that the virtual work done by the external forces (body forces and surface tractions) is equal to the virtual work of the internal stresses, i.e.,

$$\sum_{n=1}^{N} (\delta U_n - \delta W_n) = 0 \tag{1a}$$

where

$$\delta U_n = \int_{V_n} S^{ij} \delta \gamma_{ij} \, dV \tag{1b}$$

$$\delta W_n = \int_{V_n} \rho (f^i - \ddot{u}^i) \delta u_i \, dV + \int_{A_n} T^i \delta u_i dA \tag{1c}$$

In this equation, S^{ij} is the Kirchhoff stress tensor, f^i are the body forces (such as gravitational, magnetic, etc., except for

the inertial forces), T^i are the externally-applied surface tractions, γ_{ij} is the Lagrangian strain tensor, u_i are the displacement components, ρ is the mass density, and only displacement variations (δ) are permitted. Also, V_n is the undeformed volume of the nth discrete element, and A_n is the portion of the undeformed surface area of element n, over which the surface traction T^i is prescribed. The summation, Σ, extends over the total N elements of the continuum. Partial differentiation with respect to time t is denoted by (˙).

The nonlinear strain-displacement relation may be expressed as

$$\gamma_{ij} = (u_{i,j} + u_{j,i} + u_{a,i}u^a{}_{,j})/2 \tag{2}$$

where $(\,)_{,i}$ denotes covariant differentiation with respect to a Lagrangian curvilinear coordinate ξ^i using the metric tensors of the undeformed state.

If one chooses for each element an assumed displacement field of the form

$$u_i(\xi^j, t) = \lfloor N_i(\xi^j) \rfloor \{q(t)\} \tag{3}$$

where $N_i(\xi^j)$ is an appropriately assumed interpolation function and $\{q\}$ represents conveniently chosen generalized nodal displacements of the element, it follows that

$$\delta u_i = \lfloor N_i \rfloor \{\delta q\} \tag{4}$$

Hence,

$$\delta\gamma_{ij} = \lfloor D_{ij} \rfloor \{\delta q\} + \lfloor q \rfloor \{D_{ai}\} \lfloor D_j^q \rfloor \{\delta q\} \tag{5}$$

where D_{ij}, D_{ai}, and D_j^q are the appropriate associated differential operators. Employing Eqs. (4) and (5), Eq. (1) becomes

$$\sum_{n=1}^{N} \lfloor \delta q \rfloor \Big(\int_{Vn} \{D_{ij}\} S^{ij} \mathrm{d}V + \int_{Vn} \{D_{ai}\} \lfloor D_j^q \rfloor S^{ij} \mathrm{d}V \{q\} - \int_{Vn} \{N_i\} \rho f^i \mathrm{d}V - \int_{An} \{N_i\}_b T^i \mathrm{d}A + \int_{Vn} \{N_i\} \rho \lfloor N^i \rfloor \mathrm{d}V \{\ddot{q}\} \Big) = 0 \tag{6}$$

where subscript "b" is used to signify that the $\{N_i\}$ are evaluated along the element boundary.

One next proceeds to express the stresses in terms of the displacements via the stress-strain relations and the strain-displacement relations, as follows:

$$S^{ij} = E^{ijkl}(\lfloor D_{kl} \rfloor \{q\} + \lfloor q \rfloor \{D_{ck}\} \lfloor D_l^c \rfloor \{q\}/2 - \gamma_{kl}^p) \tag{7}$$

where E^{ijkl} consists of elastic constants and γ_{kl}^p represents the component of the total plastic strain (or other given initial strain). Substituting Eq. (7) into Eq. (6) (also since the element nodal generalized displacements $\{q\}$ for different elements are not completely independent, a transformation $\{J\}$ is required to relate the element nodal displacements to independent global nodal generalized displacements $\{q^*\}$ for the discrete-element assemblage), one obtains:

$$\sum_{n=1}^{N} \lfloor \delta q^* \rfloor \big([m]\{\ddot{q}^*\} + [k]\{q^*\} - \{f\} - \{f_q^{NL}\} - \{f_p^L\} - \{f_p^{NL}\} \big) = 0 \tag{8a}$$

where

$$[m] = [J]^T \int_{Vn} \{N_i\} \rho \lfloor N^i \rfloor \mathrm{d}V [J] \tag{8b}$$

$$[k] = [J]^T \int_{Vn} \{D_{ij}\} E^{ijkl} \lfloor D_{kl} \rfloor \mathrm{d}V [J] \tag{8c}$$

$$\{f\} = [J]^T \Big(\int_{Vn} \rho \{N_i\} f^i \mathrm{d}V + \int_{An} \{N_i\}_b T^i \mathrm{d}A \Big) \tag{8d}$$

$$\{f_q^{NL}\} = [J]^T \Big(- \int_{Vn} \{D_{ij}\} E^{ijkl} \langle \lfloor q \rfloor \{D_{ck}\} \lfloor D_l^c \rfloor \{q\}/2 \rangle \mathrm{d}V - \int_{Vn} \{D_{ai}\} \lfloor D_j^q \rfloor E^{ijkl} \langle \lfloor D_{kl} \rfloor \{q\} + \lfloor q \rfloor \{D_{ck}\} \lfloor D_l^c \rfloor \{q\}/2 \rangle \mathrm{d}V \{q\} \Big) \tag{8e}$$

$$\{f_p^L\} = [J]^T \int_{Vn} \{D_{ij}\} E^{ijkl} \gamma_{kl}^p \mathrm{d}V \tag{8f}$$

$$\{f_p^{NL}\} = [J]^T \int_{Vn} \{D_{ai}\} \lfloor D_j^q \rfloor E^{ijkl} \gamma_{kl}^p \mathrm{d}V \{q\} \tag{8g}$$

Performing the summation and because the variation $\{\delta q^*\}$ can be independent and arbitrary, the following equilibrium equation is obtained

$$[M]\{\ddot{q}^*\} + [K]\{q^*\} = \{F\} + \{F_q^{NL}\} + \{F_p^L\} + \{F_p^{NL}\} \tag{9}$$

where $[M]$ and $[K]$ are the usual global mass and stiffness matrix, respectively (for linear-elastic small deflection behavior), $\{F\}$ is the equivalent nodal load vector representing externally applied body forces and surface tractions, $\{F_q^{NL}\}$ represents a "generalized loads" vector arising from large deflections, $\{F_p^L\}$ and $\{F_p^{NL}\}$ are the generalized load vectors due to the presence of plastic strains and are associated, respectively, with the linear and nonlinear terms of the strain-displacement relations.

Given a set of initial conditions $\{q^*\}$ and $\{\dot{q}^*\}$ at time $t=0$, $\{F\}$ as a function of time, and the proper boundary conditions, Eq. (9) may be solved by employing an appropriate timewise finite-difference operator which provides a solution in a timewise step-by-step manner. In the present analysis, the Houbolt (4-point backward difference) operator is chosen for use. A detailed discussion of the solution procedure may be found in Ref. 22. It perhaps should be mentioned that the evaluation of $\{F_q^{NL}\}$, $\{F_p^L\}$, and $\{F_p^{NL}\}$ as in Eq. (9) involves volume integration over each discrete element of certain quantities which change with time and hence must be re-evaluated, in general, at each instant of time. For the structure undergoing large deflection, elastic-plastic behavior, it is impractical to evaluate these volume integrals analytically. Accordingly, numerical integration such as Gaussian quadrature is employed herein. This requires that the stresses and strains be evaluated at a selected finite number of Gaussian stations over the areawise and depthwise region of each element.

B. Evaluation of Stresses and Plastic Strains

A convenient way to compute the stress increment and/or plastic strain increment at any station (such as Gaussian, for example) in each element at time t_m, as discussed in Refs. 3 and 9 will be employed. Also, because the "mechanical sublayer material model"[23,24] is adopted, the only constitutive relation utilized is that for a homogenous, initially isotropic, elastic, perfectly-plastic, strain-rate dependent solid; strain hardening is automatically accommodated by this model which includes kinematic hardening and the Bauschinger effect.

It is assumed that all stresses and strains are known at time t_{m-1} and that all displacements are known at time t_m. To find the stresses $(S_j^i)_m$ at time t_m, one begins by assuming that the strain increment $(\Delta\gamma_j^i)_m$ from time t_{m-1} to time t_m is entirely elastic, and a trial (superscript T) value of stress increment is calculated from the following relation for three-dimensional behavior:

$$(\Delta S_j^i)_m^T = \frac{E}{1+\nu} \left[(\Delta\gamma_j^i)_m + \frac{\nu}{1-2\nu} (\Delta\gamma_k^k)_m \delta_j^i \right] \tag{10}$$

where E is Young's modulus, ν is Poisson's ratio and δ_j^i is the Kronecker delta. Hence, the trial stresses at time t_m are given by

$$(S_j^i)_m^T = (S_j^i)_{m-1} + (\Delta S_j^i)_m^T \tag{11}$$

Then a check is performed by substituting this trial value of the stress into the Mises-Hencky yield function,[25] Φ, to determine whether or not the trial stress state lies inside of the yield surface; thus

$$\Phi_m^T = [(S_j^i)_m^T (S_i^j)_m^T - \tfrac{1}{3}(S_k^k S_k^k)_m^T] - \tfrac{2}{3}\sigma_y^2 \tag{12}$$

where σ_y is the appropriately known uniaxial yield stress of a given mechanical sublayer of the material-behavioral model.

If $\Phi_m^T \leq 0$, the trial stress state lies within the elastic domain bounded by the yield surface. Therefore, for this time step there has been no plastic flow and the incremental deformation can be only elastic. Hence, the actual stress $(S_j^i)_m$ is equal to the trial stress; thus

$$(S_j^i)_m = (S_j^i)_m^T \tag{13}$$

and the plastic strain state is

$$(\gamma_j^i)_m^p = (\gamma_j^i)_{m-1}^p \tag{14}$$

However, if $\Phi_m^T > 0$, the trial stress lies outside of the yield surface (i.e., in the undefined region). Therefore, the trial assumption that the entire strain increment is an elastic-strain increment is not valid. Plastic flow has occurred within this time step and the actual stress state must lie on the yield surface according to the theory of perfect plasticity; then the calculation proceeds as follows. The total strain increment may be decomposed into elastic and plastic components

$$(\Delta\gamma_j^i)_m = (\Delta\gamma_j^i)_m^e + (\Delta\gamma_j^i)_m^p \tag{15}$$

Since the material is assumed to be incompressible with regard to plasticity and by the flow rule,[25] one has

$$(\Delta\gamma_j^i)_m^p = (\Delta\gamma_j^i)_m^{Dp} = (S_j^i)_{m-1}^D \lambda \tag{16}$$

where $(\Delta\gamma_j^i)^{Dp}$ is the deviatoric component of the plastic strain increment, and λ is a real nonnegative scalar quantity; also, the deviatoric component of the stress $(S_j^i)_{m-1}^D$ at time t_{m-1} is used to approximate the actual deviatoric stress value. Then the stress increment is

$$(\Delta S_j^i)_m = E/(1+\nu)[(\Delta\gamma_j^i)_m + \nu/(1-2\nu)(\Delta\gamma_k^k)_m \delta_j^i - (S_j^i)_{m-1}^D \lambda] \tag{17}$$

and the actual stress at time t_m is

$$(S_j^i)_m = (S_j^i)_{m-1} + (\Delta S_j^i)_m = (S_j^i)_m^T - (S_j^i)_{m-1}^D \tilde{\lambda} \tag{18}$$

The plastic strain at time t_m is

$$(\gamma_j^i)_m^p = (\gamma_j^i)_{m-1}^p + (S_j^i)_{m-1}^D \lambda \tag{19}$$

The quantity λ and $\tilde{\lambda}[\equiv \lambda E/(1+\nu)]$ in Eqs. (18) and (19) can be determined from the fact that $(S_j^i)_m$ must satisfy the yield condition:

$$\Phi_m = [(S_j^i)_m (S_i^j)_m - \tfrac{1}{3}(S_k^k)_m^2] - \tfrac{2}{3}\sigma_y^2 = 0 \tag{20}$$

Substituting Eq. (18) into Eq. (20) and solving for $\tilde{\lambda}$, one obtains the physically valid value

$$\tilde{\lambda} = C/[B + (B^2 - AC)^{1/2}] \tag{21}$$

where

$$A = (S_j^i)_{m-1}^D (S_i^j)_{m-1}^D - \tfrac{1}{3}(S_k^k S_k^k)_{m-1}^D \tag{21a}$$

$$B = (S_j^i)_m^T (S_i^j)_{m-1}^D - \tfrac{1}{3}(S_k^k)_m^T (S_k^k)_{m-1}^D \tag{21b}$$

$$C = \Phi_m^T = (S_j^i)_m^T (S_i^j)_m^T - \tfrac{1}{3}(S_k^k S_k^k)_m^T - \tfrac{2}{3}\sigma_y^2 \tag{21c}$$

and the following requirements must be satisfied

$$B^2 - AC \geq 0 \tag{21d}$$

$$B + (B^2 - AC)^{1/2} > 0 \tag{21e}$$

During the operation of this solution process for intensive loading problems, instances of large strain increments can occur which sometimes may lead to an imaginary or negative value of λ; that is, the conditions of Eq. (21d) and (21e) are violated. Since the time-step size for that particular instance cannot be economically reduced, a sub-increment procedure to circumvent this difficulty as discussed in Ref. 26 can be and is used.

The preceding discussion has pertained to the use of elastic, perfectly plastic rate-independent material whose yield stress is $\sigma_y \equiv \sigma_o$, the static value. However, if the yield stress is rate dependent, the same procedure applies except that the yield stress σ_y in Eqs. (12) and (20) is the strain-rate-dependent yield stress which is given approximately by[3]:

$$\sigma_y = \sigma_o(1 + |\dot{\epsilon}/D|^{1/p}) \tag{22}$$

where σ_o is the static uniaxial yield stress, D and p are material constants, and $\dot{\epsilon}$ is the uniaxial strain rate. For the three-dimensional problem, it is assumed that $\dot{\epsilon}$ of Eq. (22) may be replaced by the second invariant of the deviatoric strain-rate tensor.[3]

The discussion spanning Eq. (10) to Eq. (22) applies to any given mechanical sublayer of the material model at any spanwise or depthwise Gaussian (or checking) station in the structure. Such a procedure is applied to every mechanical sublayer of the material model at that Gaussian station.

III. Orthogonally Stiffened Quadrilateral Cylindrical Panel Element

The geometry and nomenclature of a typical quadrilateral cylindrical panel element stiffened orthogonally by longitudinal and/or circumferential stiffeners are shown in Fig. 1. The radius to the reference surface of the shell is R. The local Cartesian and the local cylindrical shell coordinate systems are (x,y,z) and (ξ,η,ζ), respectively, where the middle surface of the shell is chosen for convenience as the reference surface. Each stiffener and the basic shell panel are treated as discrete structural components.

The shell is characterized as being thin and the deformation behavior is assumed to follow the Kirchhoff-Love hypothesis. The displacement field $\tilde{u}$, $\tilde{v}$, and $\tilde{w}$ at any station in the shell may be approximated by the shell middle surface displacement u, v, and w, and rotations ϕ and ψ by:

$$\tilde{u}(\xi,\eta,\zeta) = u(\xi,\eta) - \zeta\phi(\xi,\eta) \tag{23a}$$

$$\tilde{v}(\xi,\eta,\zeta) = v(\xi,\eta) - \zeta\psi(\xi,\eta) \tag{23b}$$

$$\tilde{w}(\xi,\eta,\zeta) = w(\xi,\eta) \tag{23c}$$

where

$$\phi(\xi,\eta) = \partial w/\partial\xi \tag{23d}$$

$$\psi(\xi,\eta) = (\partial w/\partial\eta) - v/R \tag{23e}$$

To account for the strain-inducing modes and the rigid-body modes, the interpolation function selected to describe the distribution of each of these displacements throughout the

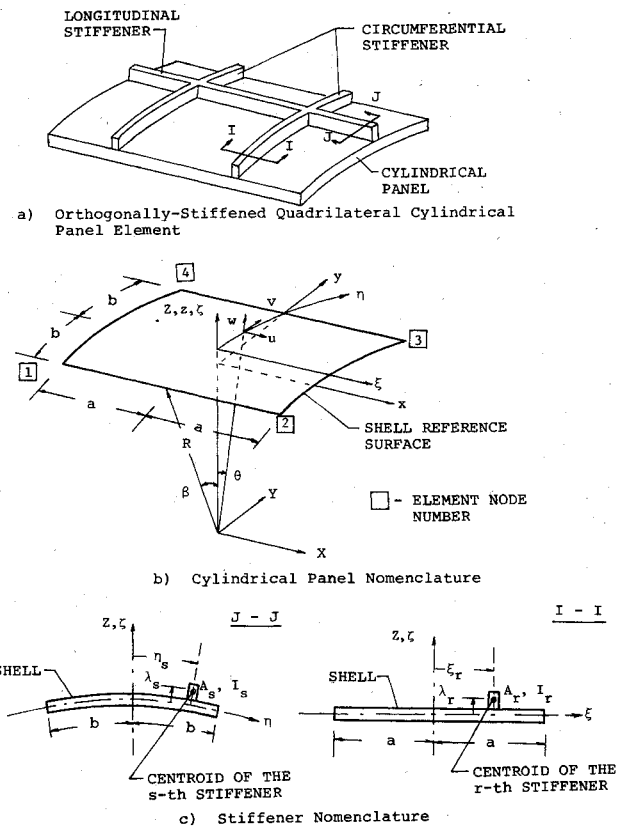

a) Orthogonally-Stiffened Quadrilateral Cylindrical Panel Element

b) Cylindrical Panel Nomenclature

c) Stiffener Nomenclature

Fig. 1 Nomenclature of an orthogonally-stiffened quadrilateral cylindrical panel element.

finite element takes the form[22]

$$u=\alpha_1+\xi\alpha_2+\eta\alpha_3+\xi\eta\alpha_4-R\sin\theta\ \alpha_6+R(\cos\theta-\cos\beta)\alpha_{10} \tag{24a}$$

$$\begin{aligned} v=&\cos\theta\ \alpha_5+\xi\cos\theta\ \alpha_6+\eta\ \alpha_7+\xi\eta\ \alpha_8-\sin\theta\ \alpha_9\\ &+\xi\sin\theta\ \alpha_{10}-R(1-\cos\theta\cos\beta)\alpha_{11}+\xi^2\alpha_{12}+\eta^2\alpha_{13}\\ &+\xi^2\eta\ \alpha_{14}+\xi\eta^2\alpha_{15}+\xi^2\eta^2\alpha_{16}+\xi^3\alpha_{17}+\eta^3\alpha_{18}\\ &+\xi^3\eta\ \alpha_{19}+\xi\eta^3\alpha_{20}+\xi^3\eta^2\alpha_{21}+\xi^2\eta^3\alpha_{22}+\xi^3\eta^3\alpha_{23} \end{aligned} \tag{24b}$$

$$\begin{aligned} w=&\sin\theta\ \alpha_5+\xi\sin\theta\ \alpha_6+\cos\theta\ \alpha_9-\xi\cos\theta\ \alpha_{10}\\ &+R\sin\theta\cos\beta\ \alpha_{11}+\xi\eta\ \alpha_{24}+\xi^2\alpha_{25}+\eta^2\alpha_{26}\\ &+\xi^2\eta\ \alpha_{27}+\xi\eta^2\alpha_{28}+\xi^2\eta^2\alpha_{29}+\xi^3\alpha_{30}+\eta^3 q_{31}\\ &+\xi^3\eta\ \alpha_{32}+\xi\eta^3\alpha_{33}+\xi^3\eta^2\alpha_{34}+\xi^2\eta^3\alpha_{35}+\xi^3\eta^3\alpha_{36} \end{aligned} \tag{24c}$$

where $\alpha_1, \alpha_2,\ldots,\alpha_{36}$ are parameters which will be expressed in terms of the generalized nodal displacements. The generalized nodal displacements which are chosen to characterize the deformation state of the element, are selected such that there are nine degrees of freedom $u,v,w,\ \phi,\ \psi,\ \partial^2 w/\partial\xi\partial\eta,\ \partial v/\partial\xi,\ \partial v/\partial\eta+w/R$, and $\partial^2 v/\partial\xi\partial\eta$ at each of the four corner nodes of the element.

With the assumptions that the shell is in a state of plane stress, the engineering component of the corresponding strain distributions may be expressed as

$$\tilde{\epsilon}_{\xi\xi}=\epsilon_{\xi\xi}-\zeta\,\kappa_{\xi\xi} \tag{25a}$$

$$\tilde{\epsilon}_{\eta\eta}=\epsilon_{\eta\eta}-\zeta\,\kappa_{\eta\eta} \tag{25b}$$

$$\tilde{\epsilon}_{\xi\eta}=\epsilon_{\xi\eta}-\zeta\,\kappa_{\xi\eta} \tag{25c}$$

where $\epsilon_{\xi\xi},\epsilon_{\eta\eta}$, and $\epsilon_{\xi\eta}$ are the midsurface inplane strains, and $\kappa_{\xi\xi},\kappa_{\eta\eta}$, and $\kappa_{\xi\eta}$ are the curvature changes. In the formulation of the present problem, the nonlinear strain-displacement relations of Sanders[27] are employed, which for the cylindrical shell may be written as:

$$\epsilon_{\xi\xi}=(\partial u/\partial\xi)+(\phi^2+\chi^2)/2 \tag{26a}$$

$$\epsilon_{\eta\eta}=(\partial v/\partial\eta)+(w/R)+(\psi^2+\chi^2)/2 \tag{26b}$$

$$\epsilon_{\xi\eta}=(\partial u/\partial\eta)+(\partial v/\partial\xi)+\phi\psi \tag{26c}$$

$$\kappa_{\xi\xi}=\partial\phi/\partial\xi \tag{26d}$$

$$\kappa_{\eta\eta}=\partial\psi/\partial\eta \tag{26e}$$

$$\kappa_{\xi\eta}=(\partial\phi/\partial\eta)+(\partial\psi/\partial\xi)+\chi/R \tag{26f}$$

where

$$\chi=(\partial u/\partial\eta-\partial v/\partial\xi)/2 \tag{26g}$$

For the plane stress case, the Mises-Hencky yield condition may be written as

$$\Phi=\sigma_{\xi\xi}^2+\sigma_{\eta\eta}^2-\sigma_{\xi\xi}\sigma_{\eta\eta}+3\sigma_{\xi\eta}^2-\sigma_y^2=0 \tag{27}$$

where σ_y is the known uniaxial yield stress of a given mechanical sublayer of the material model. The relation between stress increments and elastic increments may be assumed to be linear and to obey Hooke's law:

$$\Delta\sigma_{\xi\xi}=[E/(1-\nu^2)]\,(\Delta\tilde{\epsilon}_{\xi\xi}^{e}+\nu\Delta\tilde{\epsilon}_{\eta\eta}^{e}) \tag{28a}$$

$$\Delta\sigma_{\eta\eta}=[E/(1-\nu^2)]\,(\nu\Delta\tilde{\epsilon}_{\xi\xi}^{e}+\Delta\tilde{\epsilon}_{\eta\eta}^{e}) \tag{28b}$$

$$\Delta\sigma_{\xi\eta}=[E/2(1+\nu)]\,\Delta\tilde{\epsilon}_{\xi\eta}^{e} \tag{28c}$$

and the plastic strain increments can be established by the flow rule:

$$\Delta\tilde{\epsilon}_{\xi\xi}^{p}=\lambda(2\ \sigma_{\xi\xi}-\sigma_{\eta\eta}) \tag{29a}$$

$$\Delta\tilde{\epsilon}_{\eta\eta}^{p}=\lambda\ (2\ \sigma_{\eta\eta}-\sigma_{\xi\xi}) \tag{29b}$$

$$\Delta\tilde{\epsilon}_{\xi\eta}^{p}=\lambda\ 6\ \sigma_{\xi\eta} \tag{29c}$$

where the plastic flow parameter λ, is determined from the requirement that the actual stress state must be on the yield surface as described in Sec. II B.

For simplicity and convenience, the following assumptions are made concerning the geometry and deformation behavior of the stiffeners: 1) the stiffeners may be of material different from those of the shell to which it is attached; however, perfect bonding at each interface of the stiffener with the shell is assumed, hence, the displacements are continuous across the interfaces; 2) the stiffeners are also characterized as being thin; that is, a typical cross-section dimension of the stiffener is small compared with the radius of curvature of the shell; and 3) only the membrane and bending strains in a plane perpendicular to the shell surface and along the axial direction of the stiffener are taken into account; no contribution due to twisting strain is considered.

With these assumptions and by considering the compatibility of the displacements across the interface of the discrete stiffener and shell, the displacements within the stiffener can be determined in terms of the shell reference surface displacements (u,v,w) and rotations (ϕ,ψ) which are defined by the generalized nodal displacements at the four corner nodes of the shell element, $\{q\}$, together with the appropriate assumed-displacement interpolation functions over the element as given by Eq. (23) and (24). A detailed derivation of

the element-property matrices for the geometrically-stiffened quadrilateral cylindrical panel element may be found in Ref. 22.

IV. Description of the Experiments

The experiments involved a geometrically-stiffened clamped-edge 6061-T6 aluminum cylindrical panel configuration subjected to impulsive loading by the sheet explosive loading technique (SELT). Both transient response and permanent deformation data of high quality for use in evaluating the reliability and accuracy of methods for predicting the large-deflection elastic-plastic transient and permanent deformations of the structure, were sought.

To circumvent the difficulties that experimenters repeatedly have had in trying to achieve an ideally-clamped edge by utilizing a variety of clamping arrangements (massive serrated clamps, hardened faces, massive bolts, etc.) most of which unfortunately revealed post-test evidence of edge slippage, an "integral-edge arrangement" was attempted in the present study. This consisted, as shown in Fig. 2, of integrally machining‡ the test cylindrical panel: 6.010-in. axial length, 6.250-in. mean circumferential length (or 59.66-degree arc-span between supports), 6.002 in. mean radius, and 0.099 in. thickness; with a circumferential stiffener which has a width of 0.093 in. and a radial-direction thickness of 0.398 in, from a 2.5 in. × 13 in. × 13 in. square blank of 6061-T6 aluminum alloy. Also, although the resulting rectangular collar provided a stiff restraint to simulate an ideally-clamped edge for the cylindrical-panel test region, the specimen was in turn bolted to a 3 in.-thick 4140 annealed steel base by means of 12 high-strength 1/2-in. 13 Holo-Krome socket head shoulder screws; 3 screws were used on each side, with nuts torqued to a uniform 651 in.-lb. Note that the circumferential stiffener was also machined integrally with the basic shell structure in such a manner that the uncertainties often attending the proper modeling of stiffeners and their effective attachment to the basic structure are believed to have been minimized. Also, to reduce the hazard of undesired or premature cracking at the boundary because of stress concentrations at a sharp re-entrant corner, each corner was machined to a nominal radius of 1/8 in., which is about 25% greater than the nominal thickness of the panel.

In order to provide repeatability, confirmatory, and supplementary data, 3 stiffened clamped cylindrical panels (identified as RSCYL-1, RSCYL-2, and RSCYL-3) were tested successfully. The one test selected in the present prediction-experiment correlation assessment is specimen RSCYL-3.§ As shown in Fig. 2, the sheet of high explosive centered on the upper-surface and covering a 3 in. axial by 3.13 in. circumferential portion of the cylindrical panel was initially detonated at the center point, so that it imparts a symmetrical impulsive loading to the panel. The subsequent structural response which is also "symmetric" involves large deflections and moderate strains extending into the plastic range. The resulting detonation front in the HE sheet spread radially with a velocity of about 283,464 in./sec; hence, for all practical structural response calculation purposes, one can treat this impulsive loading as being applied simultaneously over the HE-covered portion of the test specimen. Between the sheet HE and the test specimen is a thin layer of polyurethane foam with a thickness of 1/4 in. which serves to separate the test specimen from the HE to prevent stress-wave-induced spall fracture of the test specimen following the HE detonation.

In an effort to measure transient and/or permanent strains, type EP-08-031DE-120 high elongation annealed constantan

‡This was carried out by the Whitman Tool and Die Co., Whitman, Mass., by the electrical discharge machining process in addition to conventional milling procedures.

§Specimens RSCYL-2 and RSCYL-3 were subjected to essentially identical loading; their observed transient responses and permanent deformations nearly duplicated each other.

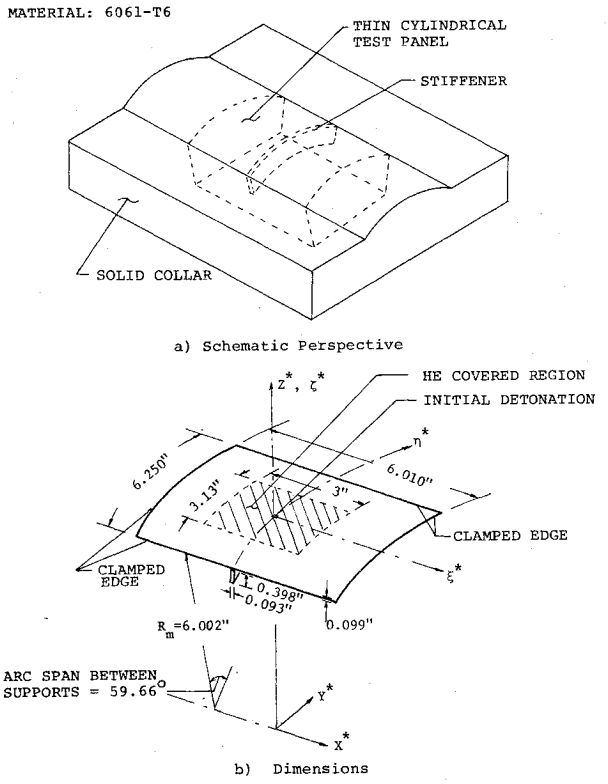

Fig. 2 Schematics and dimensions of the impulsively-loaded, integrally-stiffened clamped cylindrical panel.

foil-type polyimide-backed strain gages¶ were oriented either axially or circumferentially and attached at selected locations on the inner and the outer surface of the specimen. These gages were attached by using Micro-Measurements AE-15 cement and were cured at 175°F for 120 min, as advised by the manufacturer. According to the manufacturer, this system should permit one to measure strains (relative elongations) reliably up to about 10%. Also, in order to increase strain gage survival (because under severe impulsive loading conditions the gages may become detached from the specimen surface), a covering patch of polyimide sheet of 0.001 in. thick was cemented over the entire gage.[21] Six-ft long varnish-covered copper leads, type AWG40, were attached to each (transient strain) gage, fed to a bridge, and recorded on Tektronix oscilloscopes. These strain traces were recorded on Polaroid-type 47 film with a Tektronix 196A scope camera.

Since appropriate photographic or other equipment for measuring or recording transient deformations of structures is not available at the MIT-ASRL, only pre-test and post-test configuration measurements have been made. For a detailed description of the test specimen, experimental procedure, and results, one may consult Ref. 21. The correlation assessment between the present approximate predictions and experimental results will be discussed in the following.

V. Comparison of Predictions with Experiment

The geometry and dimensions for the impulsively-loaded clamped cylindrical RSCYL-3 panel with a circumferential stiffener are shown in Fig. 2. Taking advantage of symmetry of both the structure geometry and the external loading pattern, only one quarter of the panel with the symmetry-prescribed-displacement conditions imposed along the two "centerlines" is modeled in the present finite-element analysis by using 5 × 5 uniform meshes as depicted in Fig. 3; the five elements in the first circumferential column are circumferentially-stiffened quadrilateral cylindrical panel

¶Manufactured by the Micro-Measurements Corp., Romulus, Mich.

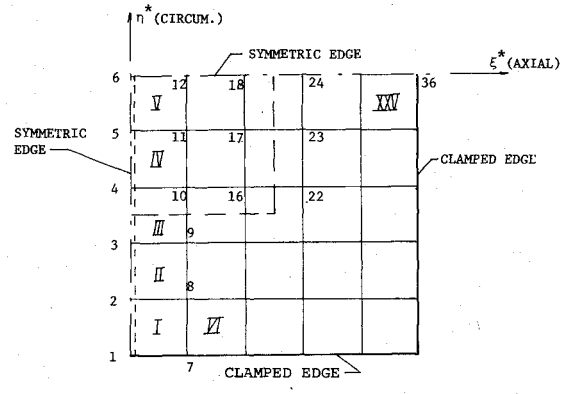

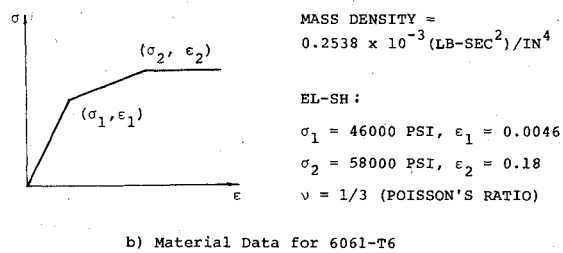

Fig. 3 Finite-element modeling and material data of the impulsively-loaded, integrally-stiffened clamped cylindrical panel.

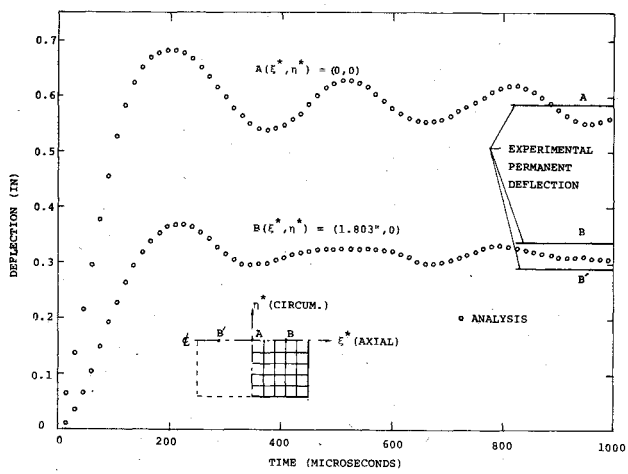

Fig. 4 Deflection response histories for the impulsively-loaded, integrally-stiffened clamped cylindrical panel.

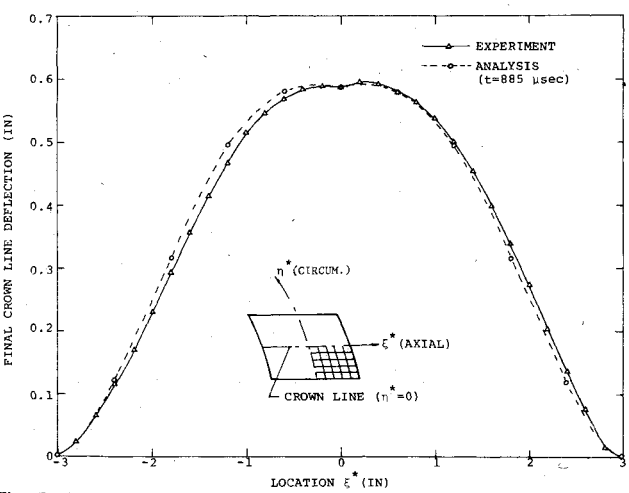

Fig. 5 Estimate of permanent crown line deformation profile for the stiffened cylindrical panel vs experiment.

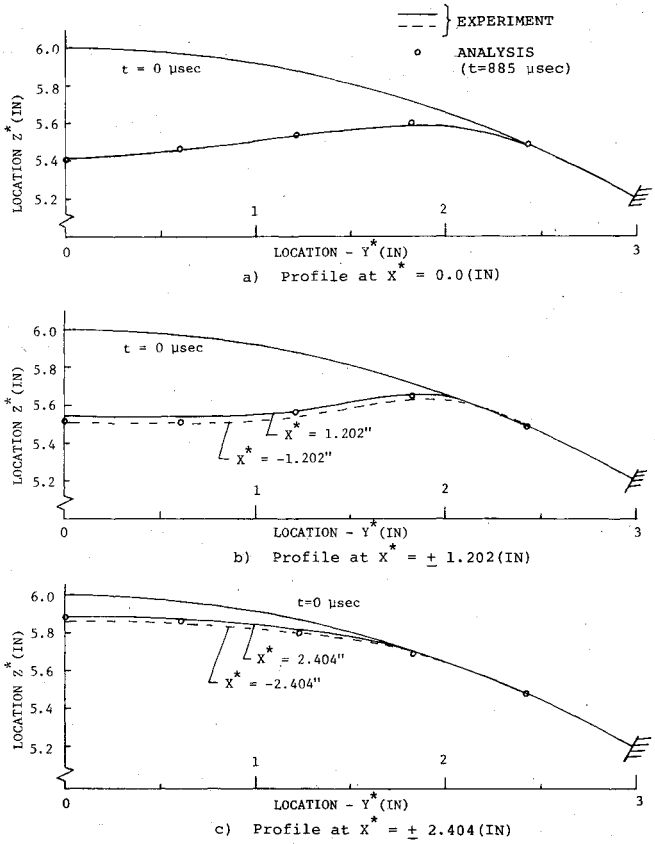

Fig. 6 Estimates of final deflection vs experiment of cross sections on the stiffened cylindrical panel.

elements and the rest are unstiffened quadrilateral cylindrical panel elements. The shell material which has a mass density per unit volume of $\rho = 0.2538 \times 10^{-3}$ lb-sec^2/in.^{4} and Poisson's ratio $\nu = 1/3$, is taken to be elastic strain-hardening (EL-SH); the uniaxial true stress-strain curve obtained from test coupons of this 6061-T6 plate material[21] was approximated by three piecewise-linear segments which are defined by two σ, ϵ pairs: $\sigma, \epsilon = 46{,}000$ psi, 0.0046; and 58,000 psi, 0.18 by the mechanical sublayer material model.

The initial conditions to be specified in the present finite-element modeling of the structure are the initial nodal transverse (radial) velocities. From impulse-calibration experimental test data described in Ref. 21, the uniform thickness sheet high explosive (HE) has a mass weight per unit area $W_e = 0.3982$ gm/in.^{2} and a specific impulse $I_s = 0.407$ (lb-sec)/gm (or 18.1×10^4 dyne-sec/gm) of HE. By equating the total impulse experienced by the structure to the impulse imparted by the sheet HE, the initial transverse velocities, $\dot{w}_o$, to be specified at nodes covered by the sheet HE for the present finite-element representation of one quadrant of the stiffened cylindrical panel are as follows: $\dot{w}_o = -6447.64$ in./sec is specified at nodes 10, 11, 12, 16, 17 and 18, and $\dot{w}_o = -3974.79$ in./sec is specified at nodes 4, 5, and 6; elsewhere the initial nodal velocity is zero.

The time-step size used in the Houbolt operator for the step-by-step time-wise numerical integration is 1.5 μsec, since this time-step has been found to be adequate to provide stable and convergent predictions for the present 5×5 finite-element mesh size. In the numerical evaluation of the integrals for determining the equivalent generalized nodal load vectors arising from large-deflection and plastic effects, nine Gaussian stations (3×3 product) for carrying out the area integration over each quadrilateral cylindrical panel element and 4 depthwise Gaussian points at each areawise Gaussian stations were used for the integration through the thickness. Also, for each stiffened panel element, 3 spanwise Gaussian stations and 4 depthwise Gaussian points at each spanwise

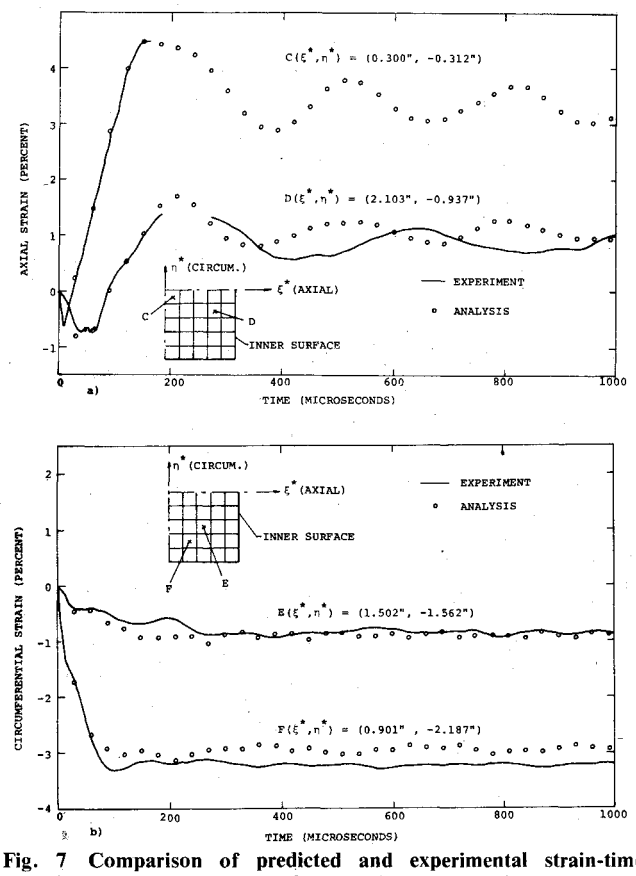

Fig. 7 Comparison of predicted and experimental strain-time histories for the impulsively-loaded, integrally-stiffened clamped cylindrical panel: a) inner surface axial strain; b) inner surface circumferential strain.

Gaussian station are used for the integration over the circumferential stiffener.

The predictions for the time history of the middle surface transverse deflection are shown in Fig. 4 for two stations: A $(\xi^*,\eta^*)=(0,0)$ and B $(\xi^*,\eta^*)=(1.803$ in.,$0)$ on crown line of the cylindrical panel (see the nomenclature of Fig. 2b). The later-time mean responses at both stations are seen to agree quite well with the experimentally measured permanent deflections which are also shown in Fig. 4 for convenient comparison . It is noted that the post-test permanent deformation of the panel shows some asymmetric behavior; this may be attributed to unintentional and/or undefined asymmetry in the initial shell geometry and/or in the applied impulsive loading. By examining the predicted time-history behavior as shown in Fig. 4, one might choose the deformation at time instant $t=885$ μsec to be a reasonable estimate of the permanent deformation condition of the panel. The resulting estimated permanent deformations are compared with those observed experimentally: 1) in Fig. 5 for the deformation profile of the panel crown-line (line at $\eta^*=0$); and 2) in Fig. 6 for the deformation profile of the cross-sections at axial stations $\xi^*=0$, 1.202 in., and 2.404 in. Very good agreement of the present predictions with experiment is observed.

Finally, the present predicted and experimentally recorded strain-time histories at 4 locations on the inner surface of the cylindrical panel are compared in Fig. 7 as a local and more sensitive comparison index. Shown in Fig. 7a are the inner surface axial strains at points $C(\xi^*,\eta^*)=(0.300$ in., -0.312 in.) and $D(\xi^*,\eta^*)=(2.103$ in.,-0.937 in.), and in Fig. 7b are the inner surface circumferential strains at points $E(\xi^*,\eta^*)=(1.502$ in., -1.562 in.) and $F(\xi^*,\eta^*)=(0.901$ in.,-2.187 in.). The present strain predictions are seen to be in reasonably close agreement with experimental records.

It should be remarked that the use of a finer finite-element space mesh in the present method should result in larger predicted transient deformations whereas the inclusion of strain rate (SR) effects should produce a smaller transient response. Therefore, the present 5×5 quarter-panel space mesh together with the present EL-SH material behavior is believed to provide a transient response preduction very close to that from the "more expensive and accurate" prediction which would result from the use of a finer space mesh (10×10, for example) together with EL-SH-SR behavior. Finally, it may be of interest to note that the 5×5 space-mesh example computed on an IBM 370/165 for 670 time steps (to $t=1005$ μsec) required 27.28 min of CPU time and 310K bytes of core storage with the present unpolished breadboard computer program.

VI. Conclusions

A finite-element formulation has been derived for hard-bonded geometrically-stiffened cylindrical shell structures, which are idealized as an assemblage of a finite number of quadrilateral panel elements. The nonlinearities resulting from both large-deflections and elastic-plastic material behavior are considered. In order to provide well-defined transient and permanent deformation data, pertinent tests of clamped-edge quadrilateral cylindrical panels, each with a circumferential stiffener and subjected to impulsive loading by the sheet explosive loading technique were carried out. The correlation assessments of the predictions in comparison with experimental measurements of transient strains as well as large permanent deformations have shown that the method of analysis presented herein is capable of providing efficient and accurate engineering predictions of transient structural responses involving large deflections and elastic-plastic material behavior.

References

[1] Witmer, E. A., Balmer, H. A., Leech, J. W., and Pian, T. H. H., "Large Dynamic Deformations of Beams, Rings, Plates, and Shells," *AIAA Journal*, Vol. 1, Aug. 1963, pp. 1848-1857.

[2] Leech, J. W., Witmer, E. A., and Pian, T. H. H., "Numerical Calculation Technique for Large Elastic-Plastic Transient Deformations of Thin Shells," *AIAA Journal*, Vol. 6, Dec. 1968, pp. 2353-2359.

[3] Morino, L., Leech, J. W., and Witmer, E. A., "PETROS 2: A New Finite-Difference Method and Program for the Calculation of Large Elastic-Plastic Dynamically Induced Deformations of General Thin Shells," MIT ASRL TR 152-1 (BRL CR 12) Dec. 1969, MIT, Cambridge, Mass.; also *Journal of Applied Mechanics*, Vol. 38, June 1971, pp. 423-436.

[4] Leech, J. W., Witmer, E. A., and Morino, L., "Dynamically-Induced Large Deformations of Multilayer, Variable Thickness Shells," *AIAA Journal*, Vol. 11, Aug. 1973, pp. 1189-1191.

[5] Pirotin, S. D., Morino, L., Witmer, E. A., and Leech, J. W., "Finite-Difference Analysis for Predicting Large Elastic-Plastic Transient Deformations of Variable-Thickness Soft-Bonded Thin Shells," MIT, ASRL TR 152-3, April 1972, MIT, Cambridge, Mass.

[6] Huffington, N. J., Jr., "Large Deflection Elastoplastic Response of Shell Structures," Rept. 1515, Nov. 1970, U. S. Army Ballistic Research Labs., Aberdeen Proving Ground, Md.

[7] Krieg, R. D. and Duffey, T. A., "UNIVALVE II: A Code to Calculate the Large Deflection Dynamic Response of Beams, Rings, Plates and Cylinders," CR-PR-68-303, Oct. 1968, Sandia Labs., Albuquerque, N. Mex.

[8] Underwood, P., "User's Guide to the SHORE Code," Rept. LMSC-D244589, Jan. 1973, Lockheed Missiles & Space Co., Palo Alto, Calif.

[9] Wu, R.W.H. and Witmer, E.A., "Nonlinear Transient Responses of Structures by the Spatial Finite-Element Method," *AIAA Journal*, Vol. II, No. 8, Aug. 1973, pp. 1110-1117.

[10] Wu, R. W. H. and Witmer, E. A., "The Dynamic Response of Cylindrical Shells Including Geometric and Material Nonlinearities," *International Journal of Solids and Structures*, Vol. 10, Feb. 1974, pp. 243-260.

[11] Stricklin, J. A., Haisler, W. E., Von Riesemann, W. A., Leick, R. D., Hunsaker, B., and Saczalski, K. E., "Large Deflection Elastic-Plastic Dynamic Response of Stiffened Shells of Revolution," TEES-RPT-72-25 and SLA-73-0218, Dec. 1972, Aerospace Engineering Dept., Texas A&M Univ., College Station, Texas.

[12] McNamara, J. F., and Marcal, P. V., "Incremental Stiffness Method for Finite Element Analysis of Nonlinear Dynamic Problems," presented at International Symposium of Numerical and Computer Methods in Structural Mechanics, Sept. 1971, Urbana, Ill.

[13] Clark, E. N., Schmitt, F. H., Ellington, D. G., Engle, I. A., and Nicolaides, S., "Plastic Deformation of Structures. I: Plastic Deformation of Beams," FDL-TDR-64-64, Vol. I, May 1965, Picatinny Arsenal, Dover, N.J.

[14] Clark, E. N. Schmitt, F. H., and Nicolaides, S., "Plastic Deformation of Structures. Part II: Plastic Deformation of Rings," FDL-TDR-64-64, Vol. 11, March 1968, Picatinny Arsenal.

[15] Krieg, R. D. and Duffey, T. A., "The Large Deflection Dynamic Elastic-Plastic Response of Clamped Beams Subjected to Explosive Loading," SC-RR-67-848, Feb. 1968, Sandia Labs., Albuquerque, N. Mex.

[16] Clark, E. N., Schmitt, F. H., and Juriaco, I. P., "Plastic Deformation of Structures. Part III: Large Plastic Deformation of Clamped Cylindrical Panels," FDL-TDR- 64-64, Vol. III, March 1968, Picatinny Arsenal, Dover, N.J.

[17] Duffey, T. A., "The Large Deflection Dynamic Response of Clamped Circular Plates Subjected to Explosive Loading," SC-RR-67-532, Aug. 1967, Sandia Labs., Albuquerque, N. Mex.

[18] Jones, N., Dumas, J. W., Giannotti, J. G., and Grassit, K. E., "The Dynamic Plastic Behavior of Shells," MIT, Dept of Ocean Engineering Rept. 71-6, April 1971, MIT, Cambridge, Mass.

[19] Jones, N., Uran, T. O., and Tekin, S. A., "The Dynamic Plastic Behavior of Fully Clamped Rectangular Plates," *International Journal of Solids and Structures*, Vol. 6, Dec. 1970, pp. 1499-1512.

[20] Witmer, E. A., Merlis, F., and Pirotin, S. D., "Experimental Studies of Explosively-Induced Large Deformations of Flat Circular 2024-0 Aluminum Plates with Clamped Edges and of Free Thin Cylindrical 6061-T6 Shells," MIT, ASRL TR 152-5 (also BRL CR 134), Jan. 1974, MIT, Cambridge, Mass.

[21] Witmer, E. A., Wu, R. W. H., and Merlis, F., "Experimental Transient and Permanent Deformation Studies of Impulsively-Loaded Rings and Cylindircal Panels, Both Stiffened and Unstiffened," MIT ASRL TR 171-3 (also AMMRC CTR 74-29), April 1974, MIT, Cambridge, Mass.

[22] Wu, R. W. H. and Witmer, E. A., "Finite-Element Predictions of Transient Elastic-Plastic Large Deflections of Stiffened and/or Unstiffened Rings and Cylindrical Shells," MIT ASRL TR 171-4 (also AMMRC CTR 74-31), April 1974, MIT, Cambridge, Mass.

[23] Prager, W. and Hodge, P. G., Jr., *Theory of Perfectly Plastic Solids*, Dover, New York, 1951.

[24] White, G. N., Jr., "Application of the Theory of Perfectly Plastic Solids to Stress Analysis of Strain Hardening Solid," Graduate Div. of Applied Mathematics, Tech. Rept. 51, Aug. 1950, Brown University, Providence, R. I.

[25] Hill, R., *Mathematical Theory of Plasticity*, Clarendon Press, Oxford, 1950.

[26] Huffington, N. J., Jr., "Numerical Analysis of Elastoplastic Stress," Memo. Rept. 2006, Sept. 1969, U. S. Army Ballistic Research Lab., Aberdeen Proving Ground, Md.

[27] Sanders, J. L., Jr., "Nonlinear Theories for Thin Shells," *Quarterly of Applied Mathematics*, Vol. 21, Jan. 1963, pp. 21-36.